A simple mixing scheme for models that resolve breaking internal waves

Jody M. Klymak*

School of Earth and Ocean Sciences, and Department of Physics and Astronomy, University of Victoria, Victoria, V8W 3P6, Canada.

Sonya M. Legg

Program in Atmosphere and Ocean Sciences, Princeton University, Princeton, NJ, 08544, USA

Abstract

Breaking internal waves in the vicinity of topography can reach heights of over 100 m and are thought to enhance basin-wide energy dissipation and mixing in the ocean. The scales at which these waves are modelled often include the breaking of large waves (10s of meters), but not the turbulence dissipation scales (centimeters). Previous approaches to parameterize the turbulence have been to use a universally large viscosity, or to use mixing schemes that rely on Richardson-number criteria.

A simple alternative is presented that enhances mixing and viscosity in the presence of breaking waves by assuming that dissipation is governed by the equivalence of the density overturning scales to the Ozmidov scale ($\varepsilon = L_T^2 N^3$, where L_T is the size of the density overturns, and N the stratification). Eddy diffusivities and viscosities are related to the dissipation by the Osborn relation ($K_z = \Gamma \varepsilon N^{-2}$) to yield a simple parameterization $K_z = \Gamma L_T^2 N$, where $\Gamma \approx 0.2$ is the flux coefficient. This method is compared to previous schemes for flow over topography to show that, when eddy diffusivity and viscosity are assumed to be proportional, it dissipates the correct amount of energy, and that the dissipation reported by the mixing scheme is consistent with energy losses in the model. A significant advantage of this scheme is that it has no tunable parameters, apart from the turbulent Prandtl number and flux coefficient. A disadvantage is that the overturning scales of the turbulence must be relatively well-resolved.

1. Introduction

There is considerable interest in how topography interacts with stratified flows to produce internal waves and turbulence. In particular the role of internal waves produced by tides and lee waves in flows over topography have been examined. In general

*Corresponding Author

Email addresses: jklymak@uvic.ca (Jody M. Klymak*), Sonya.Legg@gfdl.noaa.gov (Sonya M. Legg)

these have been treated with large-scale general circulation models (i.e. POM Merrifield and Holloway (2002) or ROMS), or with specialized non-hydrostatic codes (MITgcm Legg and Adcroft (2003), SUNTANS Venayagamoorthy and Fringer (2005)). At the other end of the spectrum LES or DNS simulations have been carried out on small scales that resolve turbulence.

Here we are interested in the scales typical of flow over deep ocean ridges, like Hawaii (Klymak et al., 2008), and at continental slopes, like Oregon (Nash et al., 2007). These flows are deep, up to 4000 m, and exhibit features on a variety of scales, from low-mode internal tides that span the whole water column, to breaking non-linear waves near abrupt changes in the topographic slopes. These breaking waves lead to density inversions that can be over 150-m tall, with dissipation rates $\varepsilon > 5\times10^{-8}$ m^2 s^{-3} in stratifications $N^2 \approx 10^{-6}$ s^{-2}. These flows have turbulent Reynolds numbers exceeding 10^6, and buoyancy Reynolds numbers $Re_b = \varepsilon/\nu N^2 > 10^4$, and Kolmogorov scales on the order of 10^{-3} m. To capture the full range of scales would require 10^6 grid cells in each dimension. Instead, to study these phenomena, we have made extensive use of a relatively efficient class of 2-D simulations that allow good resolution in the vertical (O(10m)) and horizontal (O(100 m)), such that the large-scale forcing and subsequent breaking of internal waves can be simulated. Direct numerical simulation methods are prohibitively expensive for exploration of the parameter spaces in which these phenomena are forced, therefore the turbulence dissipation in these simulations needs to be parameterized.

Two approaches to parameterizing turbulence at this scale of modelling have been used. The first is to use a high vertical viscosity $A_z \sim 10^{-2}$ m^{2}s^{-1} (Legg and Klymak, 2008) or $A_z \sim 10^{-1}$ m^{2}s^{-1} (Legg and Huijts, 2006; Legg and Adcroft, 2003). This has the benefit of being simple, and yielding the turbulence dissipation in the flow

$$\varepsilon = A_z\left(\frac{\partial \mathbf{u}}{\partial z}\right)^2 + A_h\left(\frac{\partial \mathbf{u}}{\partial x}\right)^2 + A_h\left(\frac{\partial \mathbf{u}}{\partial y}\right)^2. \tag{1}$$

As we argue below, this scheme depends strongly on the choice of A_z. Even if it is tuned to the breaking waves, it can exaggerate dissipation in the midfield where the shear is strong but not strong enough to excite shear instability or breaking.

The alternative has been schemes that have enhanced mixing based on the value of the gradient Richardson number $Ri = (\partial U_h/\partial z)^{-2}N^2$ (where U_h is the horizontal component of velocity, and N the buoyancy frequency). Some schemes depend on a critical Richardson number below which the turbulence is increased, such as the Mellor-Yamada scheme used here (Mellor and Yamada, 1982), while more recent schemes remove the necessity for a critical Richardson number (Galperin et al., 2007; Canuto et al., 2008). In all such schemes the production rate of turbulence kinetic energy is assumed to be $P = A_z(\partial U_h/\partial z)^2$ where A_z is a turbulent vertical diffusivity meant to represent unresolved eddies. The problem with these schemes in simulations with resolved breaking waves is that the turbulent eddies are partially resolved and drive overturning so that $Ri^{-1} < 0$ is resolved by the model. All the schemes introduce an arbitrarily large viscosity for negative Richardson number and ε calculated from the local shear can be unreasonably high or low, depending on this arbitrary choice.

Here we present a simple local scheme for mixing in breaking regions based on the observed correlation between the size of the convecting overturn and the Ozmidov

scale. The Ozmidov scale is related to the rate of turbulence dissipation by $\varepsilon = L_o^2 N^{-3}$. Energy arguments and observational evidence indicates that the size of convectively unstable vertical displacements in a turbulent patch L_T, is approximately equivalent to the Ozmidov scale: $L_t \approx L_o$ (Dillon, 1982; Wesson and Gregg, 1994; Moum, 1996). This brushes over significant changes in the dissipation during the life of an overturn (i.e. Gargett and Moum, 1995; Smyth et al., 2001), but is a rough average dissipation rate. The correspondence between dissipation rates and the size of overturns in convective instabilities like those found over Hawaii or in fjords appears to be robust (Klymak and Gregg, 2004; Klymak et al., 2008). We present this scheme as a bridge between large scale models that do not resolve breaking waves, and small-scale large-eddy or direct numerical simulations.

Below we implement this simple scheme whereby the turbulent viscosity A_z is calculated from the size of overturns driven by the breaking waves. We compare the energy dissipation predicted by the parameterized A_z to the energy lost from the model for the proposed scheme and compare to the constant-A_z runs and those using the Mellor-Yamada parameterization, a widely used Richardson-number scheme. Two idealized cases of interest are considered, steady and oscillating tidal flow over an obstacle.

2. Methods

The model used here is the MITgcm (Marshall et al., 1997; Legg and Klymak, 2008). We use a 2-dimensional topography, with a stretched horizontal co-ordinate system. For most of the runs here water depth $H = 2000$ m, and vertical resolution was 200 points with $\delta z_m = 10$ m; a few runs were made with $H = 1300$ and 1650 m. The horizontal domain was 174 km over 240 grid cells. The inner 80 grid cells were spaced 100 m apart, and then the grid was telescoped linearly so that for the outer cells $\Delta x = 2$ km. The obstacle in all cases is a Gaussian shape, height from the seafloor given by $h = h_m \exp(-x^2/W^2)$. The width W introduces an aspect ratio to the problem $\alpha_o = h_m/W$. The model was run in hydrostatic mode for numerical efficiency. Experiments with non-hydrostatic code did not reveal substantive differences in the features of interest here (see section 3.2 below for a comparison). That is somewhat counter-intuitive, since our proposed scheme depends on breaking waves to provide the turbulence. However, the non-hydrostatic terms in the vertical momentum equation only contribute to the evolution of the breaking, not to its actual onset. This would require a considerably more isotropic simulation grid than desirable for these scales, and would be amenable to a more isotropic mixing scheme as well. For most runs, horizontal viscosities and diffusivities were kept as low as numerically feasible, at 10^{-4} m^2 s^{-1}, except where noted.

2.1. Vertical Turbulence Schemes

Constant Viscosity. These runs compare with Legg and Huijts (2006) and Legg and Klymak (2008) who used high vertical and horizontal viscosities $A_z = 10^{-2}$ m^2 s^{-1}, and $A_H = 10^{-1}$ m^2 s^{-1}. In those papers, explicit mixing was set to zero, and handled numerically by a Superbee advection scheme (van Leer, 1979). In all our simulations shown here, the diffusivity was set to be the same as the viscosity, except for a sensitivity study that shows small differences in the dissipation due to the higher-order

scheme (section 4). The constant viscosity runs have the simple advantage that dissipation is relatively easy to compute from the flow field and local shears, and so long as the model is well-resolved, gives an accurate representation of the simulated dissipation. The disadvantage to this scheme is that the Reynolds number can be too low to allow turbulent features to develop in the first place, and that it can place too much dissipation in regions that are not expected to be turbulent.

Mellor Yamada, 2.0. The Mellor-Yamada formulation used by the MITgcm is a second-order local model. This version of the scheme does not solve a prognostic equation for the turbulent kinetic energy (so this is not to be confused with what is commonly called "Mellor-Yamada 2.5"). This scheme enhances viscosity above an arbitrary background of $A_z = 10^{-5}\mathrm{m}^2\,\mathrm{s}^{-1}$ if $Ri = N^2/S^2 < 0.25$, and viscosity becomes very high if $Ri < 0$ in density overturns (figure 1). With no capping, the maximum viscosity is $4 \times 10^{-1}\ \mathrm{m}^2\,\mathrm{s}^{-1}$. The implementation used here allows a cap to this value, adding an adjustable parameter A_{max}. The production of turbulent kinetic energy implied by this relationship between viscosity and Richardson number is the same as for the more elaborate MY2.5, but in the local scheme energy is assumed to be dissipated locally rather than propagating to remote grid cells; in this paper we refer to this as MY2.0. While we used MY2.0 rather than MY2.5 because that was the scheme already implemented in the MITgcm, it is likely that similar results would be found with MY2.5 because the production of turbulence is the same in both schemes, and this production term, rather than the diffusion and advection of TKE, is the principal difference introduced by our new scheme below. Similarly the choice of critical Richardson number has little influence on our comparison, since the flaws in the MY schemes which we are addressing here occur for $Ri < 0$.

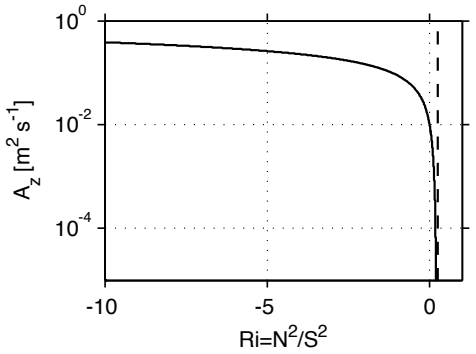

Figure 1: Mellor-Yamada 2.0 scheme used in the MITgcm. Negative Richardson numbers mean that the stratification is unstable. The dashed line is $Ri = 0.25$. The background value of $A_z = 10^{-5}\ \mathrm{m}^2\,\mathrm{s}^{-1}$.

New scheme. The high diffusivity in the MY2.0 scheme is appropriate for boundary layers, where a turbulent length scale can be calculated or estimated from similarity

theory. It is not appropriate to turbulence generated by breaking waves inside the model domain. Instead we propose a simple scheme whereby each vertical profile in the domain is sorted so there are no overturns (Thorpe, 1977) and the distance each parcel has been moved, Δz, is related to the dissipation at that location:

$$\varepsilon = (\Delta z)^2 N_S^3 \tag{2}$$

where N_S^2 is the square of the buoyancy frequency of the *sorted* profile, and should be greater than (or equal to) zero. The turbulent diffusivity is then assumed to be

$$K_z = \Gamma \varepsilon N_S^{-2} = \Gamma (\Delta z)^2 N_S \tag{3}$$

where $\Gamma = 0.2$ is the nominal flux coefficient and K_z has been estimated following Osborn (1980). The Osborn model is appropriate for turbulent mixing in flows which are overall stably stratified, as here. However, this mixing cannot take place without local overturns, and our focus here is the scenario in which these local overturns are resolved by the model, but the turbulence is not. Because the buoyancy Reynolds numbers are so large, and in the absence of compelling guidance otherwise, we then assume a turbulent Prandtl number of one, so that $A_z = K_z$.

An example of calculating ε from an oscillating tidal flow over topography is shown in figure 2. Large isopycnal displacements lead to non-linear bores at this location in the model, driving the turbulence predicted by this scheme. An example density profile has overturns (figure 2b) that correspond to vertical displacements Δz (figure 2c), yielding dissipation rates of up to $\varepsilon = 10^{-4}$ m^2 s^{-3}, in this case at the bottom of the overturn (figure 2d, thick line). Averaging these inhomogeneous events over 20 minutes yields an 80-m thick region of average dissipations close to 10^{-5} m^2 s^{-3} (figure 2d, thin line). The flow regime and turbulence levels in this model are similar to that observed at Hawaii (Klymak et al., 2008).

There are a number of objections that could be raised about this simple parameterization, and the choices of turbulent Prandtl number and flux coefficient could be refined in future. However, the goal here is to move beyond the excessive diffusivities implied by Mellor-Yamada-type schemes in overturns, or the arbitrariness of constant diffusivities. One major limitation is that this scheme does not work in well-mixed fluids where $N_S = 0$, (we are assuming that the flow is, following the Thorpe reordering, stably stratified), a second is that it does not account for shear-instabilities if they are not resolved in the model. We have also been somewhat lax in our definition of the dissipation in an overturn. The proper definition of the mean dissipation over an overturn would be $\langle \varepsilon \rangle = \Delta z^2 \langle N \rangle^3$, whereas our calculation will give $\langle \varepsilon \rangle = \Delta z^2 \langle N^3 \rangle$. It will also distribute the dissipation somewhat idiosyncratically where Δz is locally large. We do not choose to worry about these details because the correlations that are used to justify the relation between the Ozmidov scale and the Thorpe scale are poorly constrained (Moum, 1996) and the added "precision" of averaging N or ε over an overturn requires significantly more computational complexity in identifying overturning patches and performing the average. This is further justified because the variation of stratification in overturns tends to be modest (figure 2b).

The scheme is implemented on the vertical profile from each horizontal grid cell independently. A sorted profile of density is determined using a simple insertion-sort

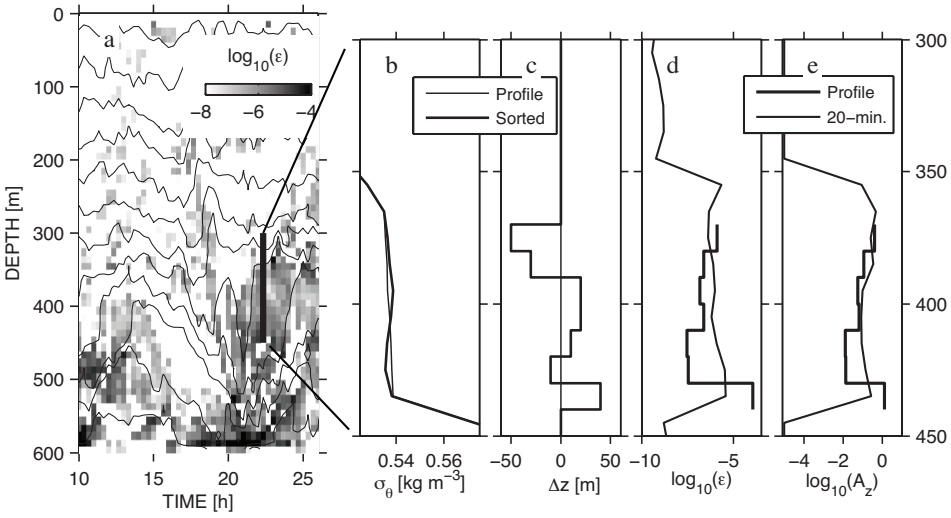

Figure 2: An example of the proposed scheme at a single location in a simulation of oscillating stratified flow over an obstacle. This is taken at $x = 2.5$ km from the simulation presented below (figure 8). a) Dissipation in the water column, with density contours over top. Density contours are from every 50 m in the background density profile. The black vertical bar indicates the profile plotted in the other panels. b) density profile between 300 and 450 m, both before and after sorting. c) vertical displacement necessary to make the profile sorted. d) Turbulence dissipation calculated for this profile (heavy line) and the 20-minute average around when this profile was taken. e) Diffusivity for this profile (heavy line) and the 20-minute average.

algorithm (Press et al., 1992). This algorithm is not well-suited to very turbulent flows, but for relatively laminar flows with rare overturns it should be faster ($\sim O(n)$, where n is the number of data points) than more advanced sorting algorithms like quicksort ($O(n \log n)$) that assume randomized data. For the simulations we are interested in here, overturns are localized to near the topography, so much of the model domain is indeed laminar. Because the sorting is local, the memory requirements are a small multiple of the number of vertical grid cells. For our model runs, this sorting step had an imperceptible effect on execution time.

3. Examples

3.1. Steady Flow over a Large Obstacle

For the first example we consider steady flow over a large obstacle, similar to model runs presented earlier (Klymak et al., 2010). Here a steady flow passes over a fixed obstacle such that $NH/U_o >> 1$, where H is the water depth, and U_o is the steady

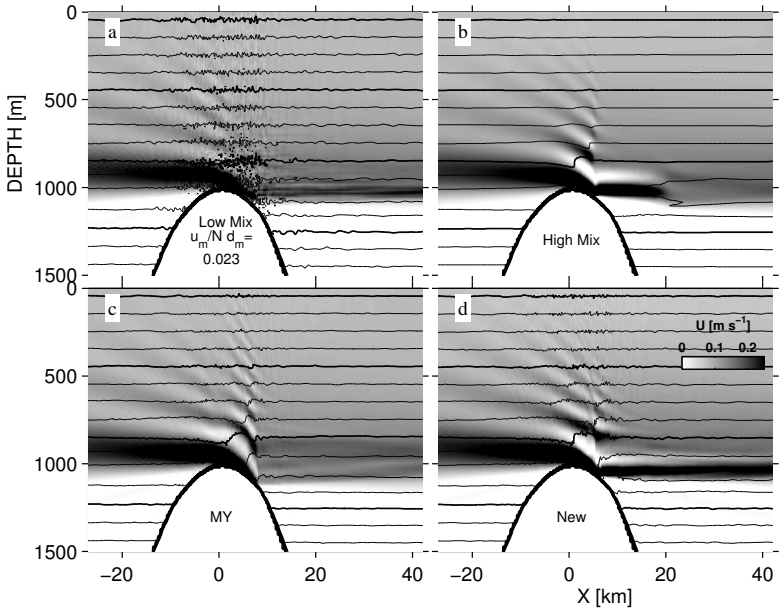

Figure 3: Velocities and density contours for four different turbulence mixing schemes used to simulate steady flow over large topography. All were run with $u_m/N(H-h_m) = u_m/Nd_m = 0.023$ a) $A_z = 10^{-5}$ m^2 s^{-1}, b) $A_z = 10^{-2}$ m^2 s^{-1}, c) local Mellor-Yamada, and d) the proposed overturning scheme.

velocity. For these runs the maximum viscosity in the Mellor-Yamada scheme was allowed to be the maximum allowed by the default parameters: $A_{max} = 0.4$ m^2 s^{-1}.

As discussed in Klymak et al. (2010), this flow is best parameterized with the barotropic flow over the ridge crest $u_m = U_o H/(H-h_m)$, where h_m is the height of the topography. For the runs here $N = 5.2\times10^{-3}$ s^{-1}, $H = 2000$ m, $H-h_m = 1000$ m, and $U_o = 0.03$ to 0.18 m s^{-1}. An example of the results for $U_o = 0.06$ m s^{-1} demonstrates the differences between the mixing schemes (figure 3,figure 4). The large-scale response is essentially the same in all four cases, with a stagnant layer forming up- and downstream of the obstacle, and acceleration of the flow above to near $u_m = 0.06$ m s^{-1}. The high-mode response is relatively similar as well, with arrested waves just downstream of the crest that have vertical wavelengths $\lambda_z \approx 2\pi\frac{u_m}{N} \approx 144$ m. There are, however, differences in the details of exactly how the high-mode response looks. The low-mixing run has a number of small scale instabilities that obscure the response, while the other three methods have differences in the exact character of the response.

The biggest difference is the dissipation in each run (figure 4). We integrate the dissipation (figure 4) for the whole water column between -25 km $< x < 25$ km, to get

$$D = \int_A \left[A_z \left(\frac{\partial \mathbf{u}}{\partial z}\right)^2 + A_h \left(\frac{\partial \mathbf{u}}{\partial x}\right)^2 \right] dA \tag{4}$$

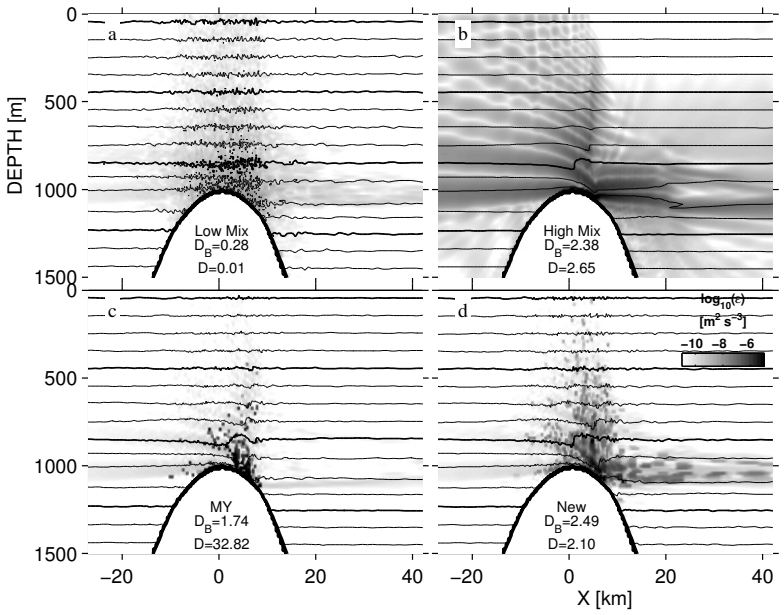

Figure 4: Example dissipation in model runs with steady stratified flow over a large obstacle. The totals are area-integrated dissipation ($[\mathrm{m}^4\mathrm{s}^{-3}]$) with D_B the difference in the Bernoulli flux past $x = \pm 25$ km, and D the reported dissipation.

The dissipation is very small for the Low-mixing case (figure 4a) and high for the Mellor-Yamada case (figure 4c), and similar for the High-mixing and New cases. The greatest difference between the High Mix case and the New case is the spatial dependence of the dissipation. The dissipation in the High Mix case is spread through the domain whereas the dissipation with the New model is localized in the jumps directly in the lee of the obstacle (figure 5). Given this, we might expect that for weaker flows the High-Mix case may start to report higher dissipation rates than the New case.

The rate at which energy is dissipated can be independently calculated from the flow. These examples are in steady state, so the dissipation of energy in the flow is

$$D_B \equiv \oint B\mathbf{u} \cdot \mathrm{d}\mathbf{A} \tag{5}$$

where $B = \frac{1}{2}\mathbf{u}^2 + P + gz$. The drop in energy flux includes both explicit dissipation, calculated as D, and unknown numerical dissipation. Therefore we have two types of inaccuracies:

- The model numerically dissipates the "right" amount D_B, but the mixing scheme does not correctly *report* this value ($D \neq D_B$).
- The model does not dissipate the "right" amount as predicted from the flow parameters (D_B incorrect).

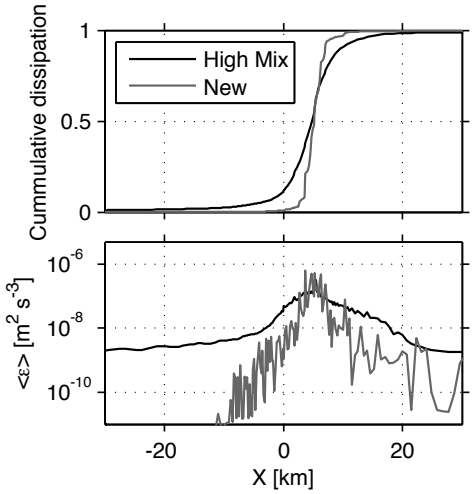

Figure 5: Dependence of the reported dissipation for the High Mix and the New dissipation schemes on horizontal location. The cumulative dissipation shows how localized the new scheme is.

Naturally we would like the mixing scheme to dissipate the "right" amount and "report" that amount accurately. The problem is that *a-priori* theories for the strength of dissipation in any flow are hard to come by, so here we resort to comparing model ensembles. In the examples above, we find that the Low Mixing case (figure 4a) has a low model dissipation D_B, and that even this low dissipation is grossly under predicted ($D < D_B$). MY2.0 has a slightly lower dissipation than High Mix and New, but it is the same order of magnitude; however it greatly over-reports the total dissipation in the model ($D > D_B$). Both High Mix and New report similar dissipations via both methods ($D \approx D_B$).

A systematic comparison over a range of resolvable u_m/Nh_m demonstrates the utility of the various schemes (figure 6). First, all the schemes dissipate roughly the same amount of energy loss through the model (D_B, figure 6a and b), with the very low mixing case ($A_z = 10^{-5}$ m^2 s^{-1}) being the prime exception. This loss of energy is because such low-viscosity runs develop small scale numerical instabilities that drain the mean flow of energy. In general the lower constant-viscosity runs have slightly lower energy losses, but the difference is not great. This constancy in the energy lost is expected in this flow regime where the energy loss is determined by the hydraulic jump in the lee of the obstacle, which is itself determined by the need of the downslope flow to match the downstream flow. Unless the mixing scheme drastically alters the response, D_B should be a constant property of the flow, and set by matching the hydraulic conditions at the obstacle crest to the downstream conditions (Baines, 1995).

The similarity of the schemes does not persist when the "reported" dissipation D is compared to the energy loss D_B (figure 6c). MY2.0 greatly over-reports the dissipation

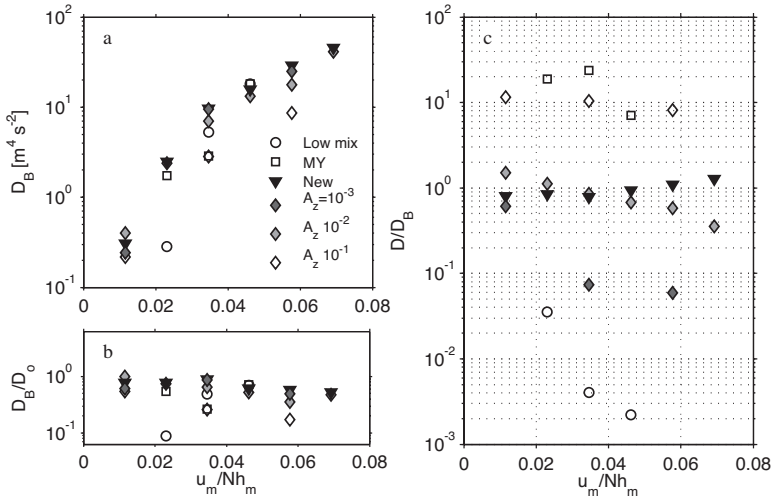

Figure 6: Comparing four different mixing schemes. a) 2-D integrated energy dissipation for different runs classified by $(Nh_m/u_m)^{-1}$, as calculated by the drop of energy over the obstacle D_B. b) The ratio of the dissipation D_B to $D_o = \frac{3}{2}\pi(H-h_m)u_m^3$, which is a relatively good scaling for this flow regime. c) The ratio of the model reported dissipation D, and the observed energy drop D_B. The "No-mixing" and "MY" runs were only made at three flow speeds.

(squares). Most of the dissipation is occurring in overturns in the lee of the obstacle (figure 4c), so $A_z \approx 10^{-1}$ m^2 s^{-1} which is too high. This leads to the energy lost from the mean flow $\varepsilon + K_z N^2 = A_z S^2$ to be over-reported because the shears are significantly reduced over a timestep; the time-scale to diffuse the 10 m shears is approximately 10 s, which is less than the 12-s timestep.

Similarly, the constant-viscosity runs can over- or under-report the dissipation (figure 6c, diamonds). If the viscosity is too low, numerical dissipation makes up the difference. If it is too high, over-reporting occurs. Note that $A_z = 10^{-2}$ m^2 s^{-1} does not do a bad job of reporting the dissipation (figure 6c, medium gray diamonds), but has a distinct trend to under-report the more turbulent runs and over-report the less turbulent ones. For this flow regime $A_z = 10^{-2}$ m^2 s^{-1} is a fortuitous choice for the constant viscosity. The distribution of vertical viscosities using the New scheme indicates why this is the case (figure 7) with the median of the PDF very near $A_z = 10^{-2}$ m^2 s^{-1}. However, as noted above, we do not feel this puts the dissipation in the right places in the water column, and it is still an arbitrary choice that would not be valid if the flow regime were different. We could improve the MY scheme with a similar tuning, but again, it would be tuning parameters for a particular regime.

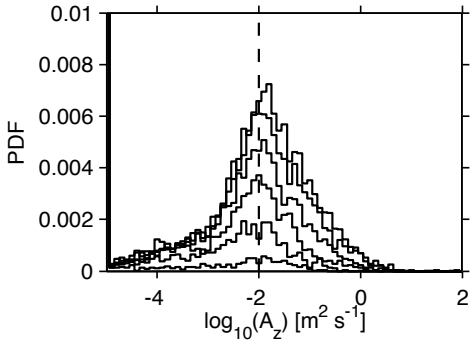

Figure 7: Distribution functions of A_z for the New mixing scheme for the steady flow over an obstacle case, with increasing flow velocities.

3.2. Oscillating flow over a Gaussian bump

The original motivation for this study was oscillating flow over a submarine ridge. Here we consider four ridges, $h_m = 300, 500, 1000$ and $1500-$ m high in $H = 2000$ m of water. All the ridges are Gaussian, with $W = 10$ km. Tidal forcing every 12.4 h on the boundaries induces $U_o = 0.04, 0.08, 0.12, 0.16, 0.20$, and 0.24 m s^{-1} barotropic flow in the deep water, and $U_T = U_o H/(H - h_m)$ barotropic flow over the obstacle. All runs were made with a constant stratification $N = 5.2 \times 10^{-3}$ s^{-1}, and carried out with the same grid configuration used for the steady case. Here we used a maximum viscosity for the MY 2.0 scheme of $A_{max} = 10^{-2}$ m^2 s^{-1}.

As above, energy is diagnosed by comparing the energy divergence in the model to the diagnosed dissipation (equation (5)). In a tidal flow this budget is never in steady state, introducing another term:

$$D_E(t) \equiv -\frac{\partial}{\partial t}\int_V E \; \mathrm{d}V + \oint B\mathbf{u}\cdot \mathrm{d}\mathbf{A}, \tag{6}$$

where $E = \frac{1}{2}\mathbf{u}^2 + gz$ is the energy density. The terms on the right hand side are large, but almost balance to give a small dissipative residual D_E, so it is imperative that these terms are diagnosed at every time step in the model, otherwise small errors in phase between two sides of the volume dominate actual divergences and good energy estimates cannot be attained. One could linearize the energy sinks and sources (i.e. by using a linear potential energy Gill, 1982), but this approach requires us to assume the energy content in the volume is in steady state, which is not true due to the background potential energy changing due to mixing. A proper available potential energy calculation (Lamb, 2008) may yield better results, but as that requires expensive global sorting, we decided that it made more sense to simply do the absolute energy balance completely.

It should also be noted that we do not reach a complete energetic steady state with these runs in six tidal periods because slow high-mode waves do not reach the edge of the control volume. The runs could be made longer, but at significant computational cost.

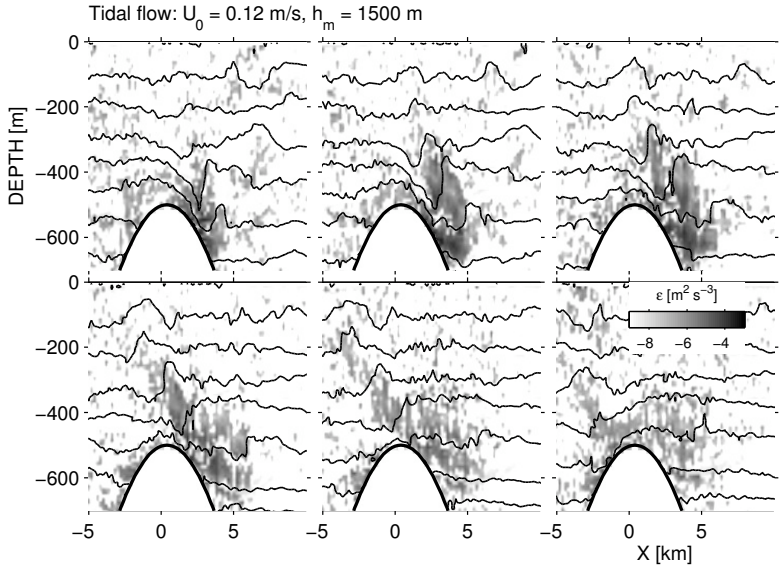

Figure 8: Hourly snapshots of energy dissipation using the New scheme for forced semi-diurnal barotropic tidal flow over a Gaussian bump. Peak flow is in the second frame in the positive-x direction.

This issue with diagnosing the energy is demonstrated in figure 9, where the difference between a fully diagnosed energy budget (a–d) and one from snapshots taken every 20 minutes (e–h) are compared for a volume that is ± 70 km from the obstacle crest. The energy fluxes into and out of this boundary are very large (though the exact magnitude depends on the definition of $z = 0$, and is therefore not unique). The difference between the energy divergence is balanced almost completely by the rate of change of energy in the volume. The residual is very small (d) and not properly represented in the 20-minute snapshots (h).

This comparison also makes the point that the high-viscosity runs do not do a very good job of tracking the energy dissipation in time (figure 9d). In contrast, the same calculation made on the new mixing scheme tracks the energy residual with time (figure 10d) more accurately, implying that the viscosity from the mixing scheme will yield useful diagnostics of energy loss.

The results over a large number of runs are similar to those attained for the steady-flow runs (figure 11). A "theoretical" dissipation, $D_T(H, h_m, U_o, N)$, is used to normalize the dissipations (and is described in a manuscript in draft); while we believe this theoretical dissipation has some usefulness, the reader is welcome to consider it a scaling that happens to agree with our New overturn-based dissipation. However, it is clear that using constant viscosities $A_z = 10^{-2}$ and 10^{-1} m^2 s^{-1} yields dissipations that depend on the value of the viscosity (figure 11a–f). As in the steady case, the reported dissipations (D, figure 11a–c) have the greatest variation, whereas the energy loss in

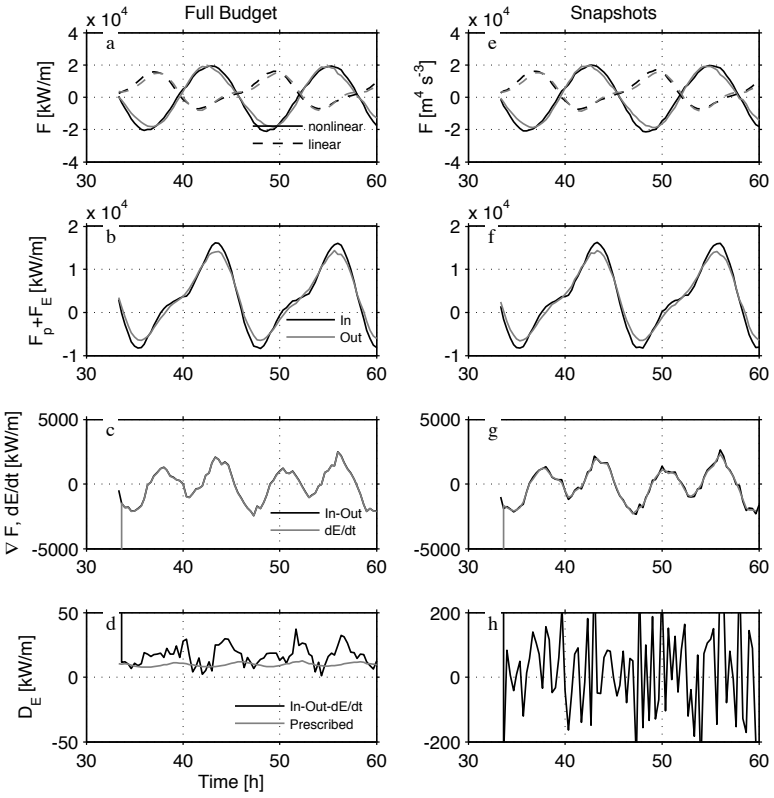

Figure 9: Time series of energy budget for a volume between $x = \pm 70$ km using constant $A_z = 10^{-2}$ m^{2}s^{-1}. a–d) are using a full budget diagnosed at every time step of the simulation, while e–h) is the same budget from snapshots taken every 20 minutes (37 times a tidal period). a) and e) are the linear (dashed) and non-linear (solid) energy fluxes, the two lines representing the in- and out-going fluxes. b) and f) is the total flux. c) and g) are the flux divergences compared to the rate of change of energy in the volume; these two values lie almost one atop the other. d) and h) is the difference between the energy flux divergence and the energy change in the volume (solid) compared with the prescribed dissipation (gray). Note the difference in scale between d) and h).

the model (D_E, figure 11d–f) tends to be more constant. Unlike the steady runs, the MY2.0 scheme tends to under-report the dissipation in the oscillating runs.

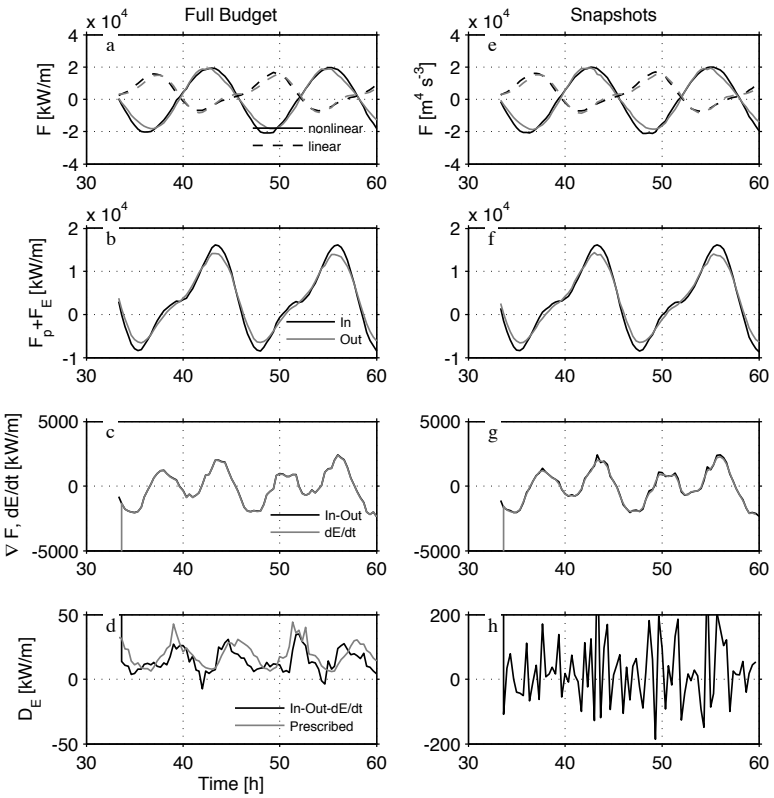

Figure 10: As for figure 9 except for the overturning-based dissipation proposed here. Again, note that d) and h) are different scales.

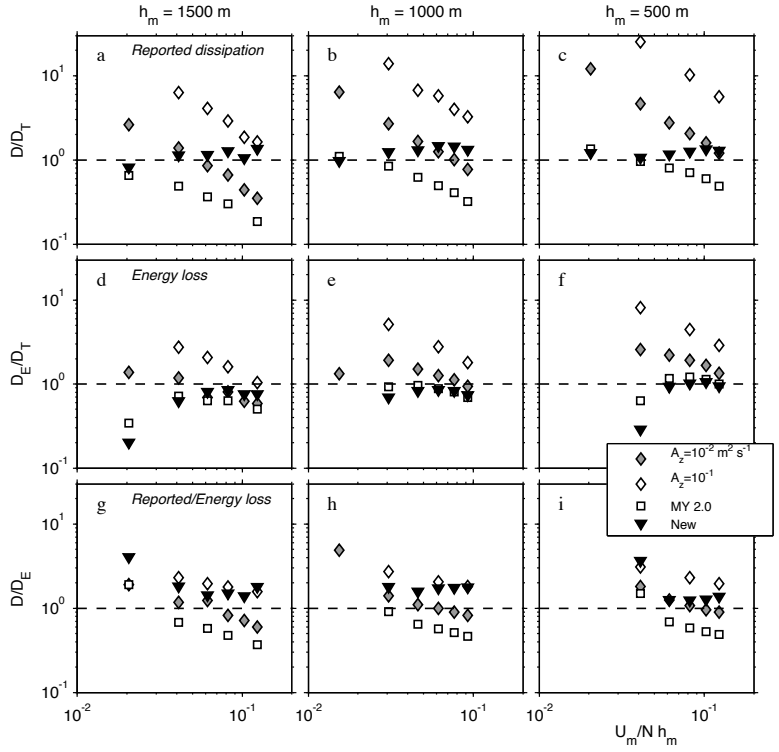

Figure 11: Dissipation in tidal runs for different mixing schemes: a–c) dissipation reported by the viscocity D, compared to a theoretical estimate of the dissipation D_T. d–f) dissipation calculated from an energy budget D_E. g–i) The ratio of reported dissipation to diagnosed dissipation: D/D_E.

The mixing scheme proposed here has the best characteristics of the schemes tested. It underestimates the dissipation slightly for the smallest (and thus least turbulent) ridge (figure 11d), and overestimates slightly for the most turbulent (figure 11f). The size of the lee waves that drive much of the turbulence can be estimated from the tidal flow and stratification as $\lambda_0 = 2\pi U_T/N$. If there is insufficient resolution in the model to resolve these waves then there is little hope they will break and be well-represented by the mixing scheme.

Again, the differences in where the dissipation takes place are the same as for the steady flow case: the high-viscosity spreads the dissipation out over a larger region where tidal energy creates shears in the flow (figure 12a,b). These shears, however, are stable to shear instabilities ($Ri > 0.25$), and therefore do not produce extra dissipation in the MY2.0 (figure 12c,d) or the new mixing scheme (figure 12e,f). All three schemes predict strong mixing in the lee of the obstacle during both phases of the tide.

As a final note, we tested the importance of hydrostaticity for the New mixing scheme in these simulations (figure 13). For both reported dissipation and the energy

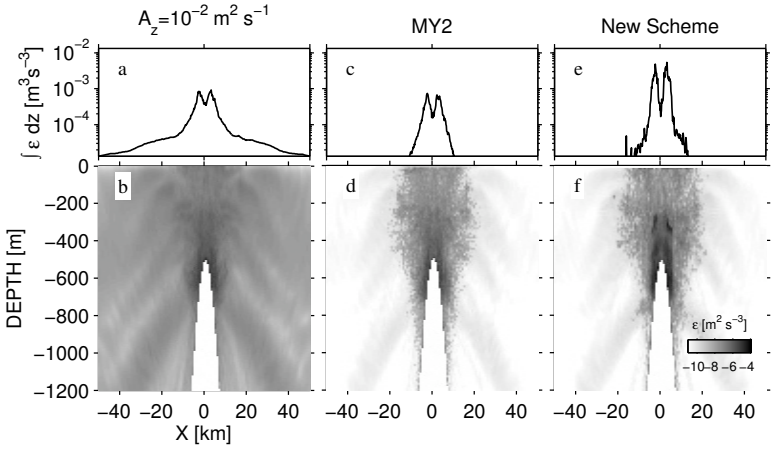

Figure 12: Mean dissipation over a tidal period for $U_t = 0.16\ \mathrm{m\,s^{-1}}$, $h_m = 1500$ m, and $N = 5.2 \times 10^{-3}\ \mathrm{s^{-1}}$ for three mixing schemes. Upper panels (a,c,e) are depth integrals of the dissipation as a function of distance from the obstacle.

divergence, the response was almost identical for the model run in hydrostatic and non-hydrostatic configurations. The differences did seem to be larger for larger forcing (figure 13e,f), perhaps indicating that the dynamics inside the larger breaking waves were playing a role, however, the time-smoothed averages were not significantly different. Note again, that the model has a 10:1 aspect ratio in the grid cells near the obstacle, so the lack of strong non-hydrostatic effects is not surprising. Experiments with more horizontal resolution may turn up more substantive differences, but again, such simulations could be made with a more isotropic mixing model that acts on the turbulent scales themselves.

4. Resolution and Advection-Scheme Limitations

The MITgcm, or any numerical model that we know of, does not explicitly try to conserve mechanical energy, so the ability to attain near-balances as we have attempted to show above, is encouraging. There are a number of limitations to the new scheme (and the other schemes) that should be accounted for, and we attempt to discuss them here.

First, the energy dissipation depends somewhat on the advection scheme used. Most of the runs in this paper were made with a simple and efficient second-order scheme. This scheme is quite noisy, and some of this noise goes into producing extra dissipation in the model. This is seen most clearly when considering the resolution dependence of all the schemes (figure 14). Here the same runs were made with finer resolutions. All the schemes demonstrate more dissipation as the resolution is increased. However, the New scheme does so more precipitously. A 2.5-m resolution run shows

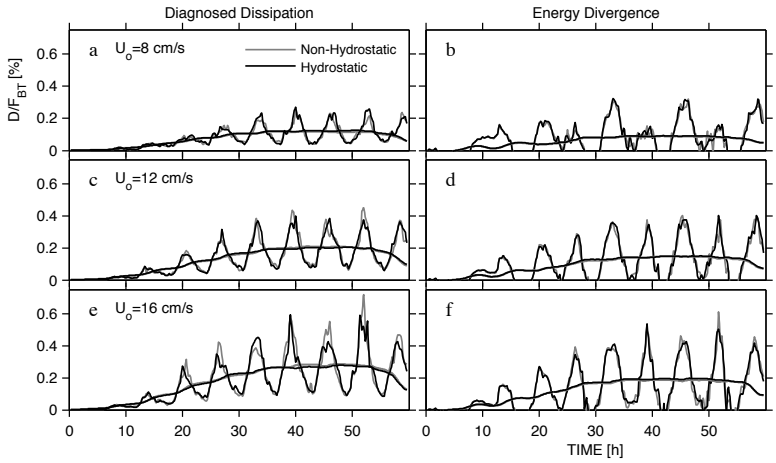

Figure 13: Comparison of hydrostatic and non-hydrostatic dissipation and energy loss from three forcings over a Gaussian obstacle.

even more dissipation, indicating that increasing vertical resolution makes the dissipation grow too much. It is relatively difficult to tell what causes the extra dissipation, but it is not just a simple reporting error as it shows up in both D and D_E. We suggest that the extra dissipation is occurring because finer resolution allows more noise to develop due to inaccuracies in the advection scheme, which makes more overturns and therefore more dissipation. The constant-viscosity simulations also have increased dissipation with resolution, but the increase is smaller.

If we use a nonlinear limited advection scheme (figure 14b), in this case the Superbee flux-limited scheme, we find that the increase in dissipation with increased resolution is almost the same as the constant-viscosity runs. However, the solutions are smoother and the dissipation driven by overturns is now somewhat lower than before for the base 10-m runs.

We consider the difference in dissipations in the New scheme more systematically with a set of experiments of tidal flow over a ridge using the nominal 10-m resolution (figure 15). In general, the second-order scheme has higher dissipations than the flux-limiting scheme for all dissipations, with the second order scheme over-reporting the dissipation (figure 15a, circles) and the Superbee scheme under-reporting (figure 15a, diamonds). The two schemes tend to dissipate the same amount of energy from the model (D_E, figure 15b) except for the least-turbulent flows, where the Superbee scheme removes more energy from the flow than the 2-nd order. This is consistent with the Superbee scheme having some additional numerical diffusion.

As mentioned above, the mixing scheme and the simulations have a natural limit where the vertical resolution becomes too coarse to resolve the waves in the lee of the obstacle.

Figure 14: Comparison of dissipations at different vertical resolutions with a) 2-nd order centered advection scheme, and b) Superbee advection scheme. The triangle in each panel is for 2.5-m vertical resolution.

5. Summary

We have presented a simple mixing scheme for models that resolve breaking internal waves based on the Ozmidov scale implied by these breaking waves. We expect this scheme will be the most useful for parameterizing mixing in strong flows over topography, with particular application to internal tide generation and reflection problems. It may also be useful for mean-flows over rough topography such as might occur in the Antarctic circumpolar current.

There is a slight cost to the scheme in terms of memory and processor time. The sorting algorithm should be relatively cheap except for very turbulent flows.

We have used some simplifying assumptions that are common in the literature such as that the Prandtl number is one and that the flux coefficient Γ is a constant. There is significant interest in if these assumptions are valid (i.e. Gargett and Moum, 1995; Smyth et al., 2005, 2001) that is beyond the scope of our study here.

The major limitation of our new mixing scheme is that the largest mixing events should be driven by breaking waves rather than unresolved shear instabilities. For instance, in the tidal mixing over the Knight Inlet sill there is clear evidence of both shear instability and breaking in the lee wave (Farmer and Armi, 1999; Klymak and Gregg, 2004). For the flows discussed in this paper resolved shear instability was very rare; the Mellor-Yamada mixing was almost always maximized, indicating that it was responding to convective instability, rather than high shears (figure 12). However, if a flow was being considered where shear instability was also thought to be important, such as larger-scale overflows (Legg et al., 2009), it would be very easy to make a hybrid mixing scheme that also enhanced mixing in shear layers. Rather than the profile in figure 1, one could imagine the same profile for $Ri > 0$ and then an abrupt transition to the overturning mixing for negative Richardson Numbers. Alternate shear-driven schemes, such as that proposed by Jackson et al. (2008), could also be added.

The authors thank Alistair Adcroft for helpful comments on a draft of this paper, and two anonymous reviewers and Boris Galperin for their very helpful comments on the submitted version. JK was supported by ONR grants N00014-08-1-

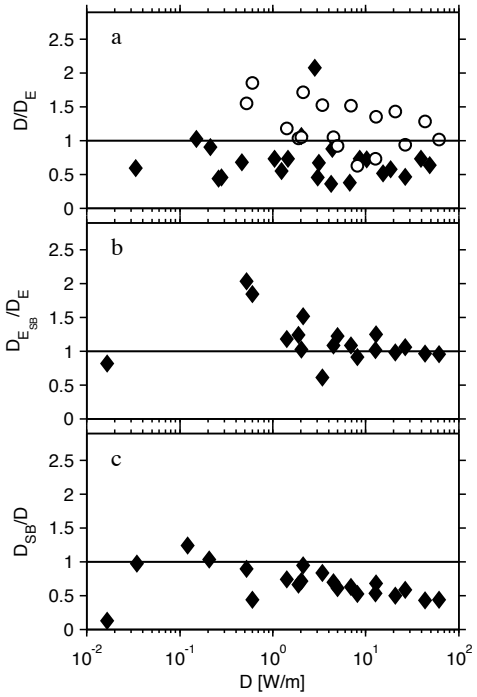

Figure 15: Dependence of dissipation on advection scheme for 10-m resolution oscillating flow over an obstacle: a) dissipation compared with energy divergence for 2nd-order scheme (circles) and superbee advection scheme (diamonds). The superbee scheme tends to have some of its dissipation go unreported, the 2-nd order scheme over-reports its dissipation. b) the ratio of energy divergences in the models. Both schemes lose approximately the same amount of energy except at low dissipations where the superbee scheme dissipates more. c) Because it under-reports, the superbee scheme has less dissipation than the 2-nd order scheme.

0376 and N00014-08-1-0274 and NSERC grant 327920. SL was supported by award NA08OAR4320752 from the National Oceanic and Atmospheric Administration, U.S. Department of Commerce. The statements, findings, conclusions, and recommendations are those of the author(s) and do not necessarily reflect the views of the National Oceanic and Atmospheric Administration, or the U.S. Department of Commerce.

References

Baines, P. G., 1995. Topographic Effects in Stratified Flows. Cambridge Univ. Press, New York.

Canuto, V., Cheng, Y., Howard, A., Esau, I., 2008. Stably stratified flows: a model with No Ri (cr). Journal of the Atmospheric Sciences 65 (7), 2437–2447.

Dillon, T. M., 1982. Vertical overturns: A comparison of Thorpe and Ozmidov length scales. J. Geophys. Res. 87, 9601–9613.

Farmer, D. M., Armi, L., 1999. Stratified flow over topography: The role of small scale entrainment and mixing in flow establishment. Proc. R. Soc. London, Ser. A 455, 3221–3258.

Galperin, B., Sukoriansky, S., Anderson, P., 2007. On the critical Richardson number in stably stratified turbulence. Atmospheric Science Letters 8 (3), 65.

Gargett, A. E., Moum, J. N., 1995. Mixing efficiencies in turbulent tidal fronts: Results from direct and indirect measurement of density flux. J. Phys. Oceanogr. 25, 2583–2608.

Gill, A. E., 1982. Atmosphere-Ocean Dynamics. Academic.

Jackson, L., Hallberg, R., Legg, S., 2008. A parameterization of shear-driven turbulence of ocean climate models. J. Phys. Oceanogr. 38, 1033–1053.

Klymak, J. M., Gregg, M. C., 2004. Tidally generated turbulence over the Knight Inlet sill. J. Phys. Oceanogr. 34 (5), 1135–1151.

Klymak, J. M., Legg, S., Pinkel, R., 2010. High-mode stationary waves in stratified flow over large obstacles. J. Fluid Mech. 644, 312–336.

Klymak, J. M., Pinkel, R., Rainville, L., 2008. Direct breaking of the internal tide near topography: Kaena Ridge, Hawaii. J. Phys. Oceanogr. 38, 380–399.

Lamb, K. G., 2008. On the calculation of the available potential energy of an isolated perturbation in a density stratified fluid. J. Fluid Mech. 597, 415–427.

Legg, S., Adcroft, A., 2003. Internal wave breaking at concave and convex continental slopes. J. Phys. Oceanogr. 33, 2224–2246.

Legg, S., Briegleb, B., Chang, Y., Chassignet, E., Danabasoglu, G., Ezer, T., Gordon, A., Griffies, S., Hallberg, R., Jackson, L., et al., 2009. Improving oceanic overflow representation in climate models: the Gravity Current Entrainment Climate Process Team. Bulletin of the American Meteorological Society 90 (5), 657–670.

Legg, S., Huijts, K. M., 2006. Preliminary simulations of internal waves and mixing generated by finite amplitude tidal flow over isolated topography. Deep Sea Research Part II: Topical Studies in Oceanography 53 (1-2), 140 – 156.

Legg, S., Klymak, J. M., 2008. Internal hydrualic jumps and overturning generated by tidal flow over a steep ridge. J. Phys. Oceanogr., 1949–1964.

Marshall, J., Adcroft, A., Hill, C., Perelman, L., Heisey, C., 1997. A finite-volume, incompressible Navier-Stokes model for studies of the ocean on parallel computers. J. Geophys. Res. 102 (C3), 5753–5766.

Mellor, G. L., Yamada, T., 1982. Development of a turbulence closure model for geophysical fluid problems. Rev. Geophys. Space Phys. 20, 851–875.

Merrifield, M. A., Holloway, P. E., 2002. Model estimate of m_2 internal tide energetics at the Hawaiian Ridge. J. Geophys. Res. 107 (C8), 10.1029/2001JC000996.

Moum, J. N., 1996. Energy-containing scales of turbulence in the ocean thermocline. J. Geophys. Res. 101 (C6), 14095–14109.

Nash, J., Alford, M., Kunze, E., Martini, K., Kelley, S., 2007. Hotspots of deep ocean mixing on the Oregon continental slope. Geophys. Res. Lett. 34, L01605, doi:10.1029/2006GL028170.

Osborn, T. R., 1980. Estimates of the local rate of vertical diffusion from dissipation measurements. J. Phys. Oceanogr. 10, 83–89.

Press, W. H., Teukolsky, S. A., Vetterling, W. T., Flannery, B. P., 1992. Numerical Recipes in C, 2nd Edition. Cambridge Univ. Press, Cambridge, U. K.

Smyth, W. D., Moum, J. N., Caldwell, D. R., 2001. The efficiency of mixing in turbulent patches: Inferences from direct simulations and microstructure observations. J. Phys. Oceanogr. 31, 1969–1992.

Smyth, W. D., Nash, J., Moum, J., 2005. Differential diffusion in breaking Kelvin-Helmholtz billows. J. Phys. Oceanogr. 35, 2753–2766.

Thorpe, S. A., 1977. Turbulence and mixing in a Scottish loch. Phil. Trans. Roy. Soc. London, Ser. A 286, 125–181.

van Leer, B., 1979. Towards the ultimate conservative difference scheme. J. Comput. Phys. 32, 101–136.

Venayagamoorthy, S. K., Fringer, O. B., 2005. Nonhydrostatic and nonlinear contributions to the energy flux budget in nonlinear internal waves. Geophys. Res. Lett. 32 (L15603).

Wesson, J. C., Gregg, M. C., May 1994. Mixing at Camarinal Sill in the Strait of Gibraltar. J. Geophys. Res. 99 (C5), 9847–9878.